arXiv:1406.5423v1 [cond-mat.str-el] 20 Jun 2014

Tunneling Spectroscopy Across the Superconductor-Insulator Thermal Transition

Sabyasachi Tarat and Pinaki Majumdar
Harish-Chandra Research Institute, Chhatnag Road, Jhusi, Allahabad 211019, India
(Dated: 11 June 2014)

Advances in scanning tunneling spectroscopy reveal the presence of superconducting nanoregions well past the bulk thermal transition in strongly disordered superconductors. We use a Monte Carlo tool to capture the spatially differentiated amplitude and phase fluctuations in such a material and establish spatial maps of the coherence peak as the superconductor is driven through the thermal transition. Analysis of the local density of states reveals that superconducting regions shrink and fragment with increasing temperature, but survive in small clusters to a temperature $T_{clust} \gg T_c$. The gap (or pseudogap) in the spectrum survives in general to another independent scale, T_g, depending on the strength of interaction. This multiple scale description is consistent with recent measurements and defines the framework for analysing strongly disordered superconductors.

Although superconductors with s-wave symmetry are robust to weak non-magnetic disorder [1, 2], moderate disorder can lead to large inhomogeneities in the pairing amplitude, and strong phase fluctuation between the 'islands' that emerge. This suppresses the transition temperature, and beyond a critical disorder the ground state becomes insulating [3]. While the bulk features of the superconductor-insulator transition (SIT) have been explored experimentally for several decades [4–7], the recent use of high resolution scanning tunneling spectroscopy (STS) [8–15] has generated new questions about the superconducting state near the SIT.

The experiments allow two major advances. (i) They confirm the essentially inhomogeneous nature [8–15] of the superconducting (SC) state, affirming that one does not have a homogeneous suppression of SC order with disorder and temperature. (ii) They highlight the presence of *additional temperature scales* in the problem, for example, a cluster formation scale, T_{clust}, a pseudogap formation scale, T_{pg}, and, at strong disorder, a possible gap formation scale T_g - all distinct from T_c. In addition, STS measurements quantify the detailed behaviour of the local density of states (LDOS) with disorder and increasing temperature [8, 10, 12–15] - posing a challenge for theories that address only average properties.

Addressing these issues calls for an approach that captures the increasing fragmentation in the ground state and retains the crucial phase and amplitude fluctuations that dictate thermal properties. Mean field Hartree-Fock-Bogoliubov-de-Gennes (HFBdG) theory [16] reasonably describes the ground state but ignores phase fluctuations, while quantum Monte Carlo (QMC) [17, 18] retains all fluctuations but lacks spatial resolution. Using an auxiliary field scheme that captures the HFBdG ground state, and the correct T_c and critical disorder (V_c), we provide a spatially resolved description of the thermal transition and estimate the emergent scales in a strongly disordered superconductor.

Working at moderate interaction ($U = 2t$, see later) we confirm the fragmentation of the superconducting ground state with increasing disorder, with SC islands surviving in an 'insulating' background. Our key results on thermal behaviour of the LDOS are the following: (i) At weak disorder increasing temperature (T) leads to spatially homogeneous closure of the gap at T_c. For $V \to V_c$ the $T = 0$ gaps are lower in the SC regions than in the insulator, increasing T reduces all gaps but they survive to a scale $T_g \gg T_c$, and a pseudogap is observed to $T_{pg} \gg T_g$. (ii) In the weakly disordered system the coherence peak in the LDOS vanishes throughout the system at $T = T_c$. At strong disorder it survives on isolated clusters to a scale $T_{clust} \gg T_c$. (iii) The scales T_g, T_{clust}, *etc*, have distinct physical origin. We establish their variation with disorder and interaction strength. Finally, (iv) we suggest a simple lattice Ginzburg-Landau model, with parameters extracted from the electronic problem, that reasonably describes the complex thermal behaviour.

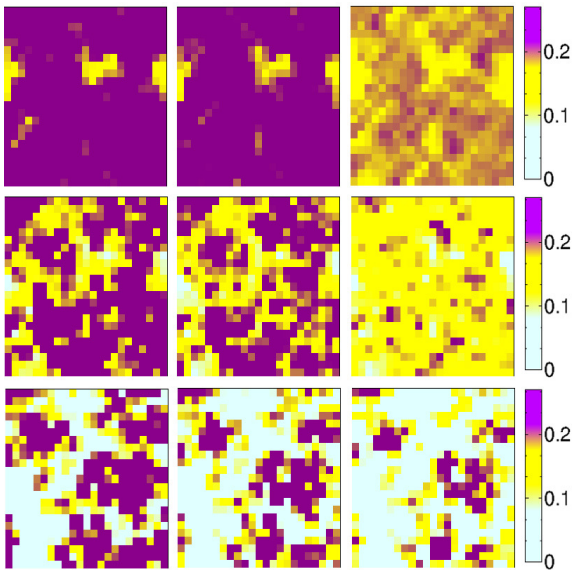

FIG. 1. Colour online: Maps of the tunneling conductance integrated over a narrow frequency window around the coherence peak feature in the LDOS (see text). Rows, top to bottom, $V = 0.2V_c, 0.5V_c, 0.9V_c$. Columns, left to right, $T/T_c(V) = 0, 0.5, 1.0$. Thermal average over 100 configurations.

We study the attractive two dimensional Hubbard model (A2DHM) in the presence of potential scattering: $H = H_{kin} + \sum_{i\sigma}(V_i - \mu)n_{i\sigma} - |U|\sum_i n_{i\uparrow}n_{i\downarrow}$ with $H_{kin} = -t\sum_{\langle ij\rangle\sigma} c^\dagger_{i\sigma}c_{j\sigma}$. t is the nearest neighbour tunneling amplitude. V_i is a random potential picked from a normalised flat distribution between $\pm V$. μ is the chemical potential controlling the electron density n. We fix μ so that $n \approx 0.9$. $U > 0$ is the strength of onsite attraction. We will set $t = 1$ and measure all energies, and temperature (T), in units of t. We set $U = 2t$, to be close to the experimentally relevant weak coupling window.

The difficulty of the A2DHM lies in handling the interaction term. We use a decomposition [19, 22, 23] of the interaction in terms of a pairing field, $\Delta_i = |\Delta_i|e^{i\theta_i}$, and a density field ϕ_i and treat these fields as classical. This leads to the effective Hamiltonian $H_{eff} = H_{kin} + \sum_{i\sigma}(V_i - \mu)n_{i\sigma} + H_{coup} + H_{cl}$, where $H_{coup} = \sum_i(\Delta_i c^\dagger_{i\uparrow}c^\dagger_{i\downarrow} + h.c) - \sum_i \phi_i n_i$ and $H_{cl} = \frac{1}{U}\sum_i(|\Delta_i|^2 + \phi_i^2)$. We solve the coupled fermion-auxiliary field problem through a Monte Carlo [19–21]. At finite T this allows us to consider electron propagation in an amplitude and phase fluctuating background, affording a dramatic improvement in the handling of thermal physics. We have discussed the method in detail elsewhere [22, 23] so we move on to the results.

The 'clean T_c' at $U = 2t$ is $T_c^0 \approx 0.07t$. Increasing disorder pushes our T_c below measurement resolution ($\sim 0.005t$) at $V \approx 2t$. We set this as V_c [24]. Based on the bulk transport and spectral properties, we characterise [22] $V \lesssim 0.25V_c$ as 'weak' disorder, $0.25V_c \lesssim V \lesssim 0.75V_c$ as intermediate, and $V \gtrsim 0.75V_c$ as strong disorder. The weak disorder regime is characterised by a featureless DOS and metallic transport for $T > T_c$, intermediate disorder involves a pseudogap (PG) for $T > T_c$ and a thermal crossover from insulating to metallic resistivity, while strong disorder involves a hard gap over a window $T_g > T > T_c$ and activated transport at high T.

Fig.1 presents a summary of the thermal evolution of the coherence peak map at weak, moderate, and strong disorder. Our data shows the integrated tunneling conductance (TC) over the window $[\omega_c^-, \omega_c^+]$, defined by $T_i^{coh} = \langle\int_{\omega_c^-}^{\omega_c^+} d\omega N_{ii}(\omega)\rangle$, where $N_{ii}(\omega)$ is the local density of states at site $\mathbf{R}_i$. $\omega_c^- = 0.2t$ and $\omega_c^+ = 0.45t$ are chosen so that they cover the coherence peaks in the global density of state, and hence gives information about the local phase correlations in the system.

We make the following observations: (a) At weak disorder the pattern remains almost homogeneous at all T, except for a few isolated regions. Coherence peaks get suppressed with increasing temperature, and vanish by $T = T_c$. (b) At intermediate disorder the ground state is noticeably inhomogeneous and increasing T causes further fragmentation. However, by the time $T = T_c$ hardly any coherence peaks are visible anywhere. (c) The high disorder regime shows tenuously connected clusters at $T = 0$, which shrink as T is increased, but have a prominently visible but disconnected pattern at $T = T_c$. In fact at $V = 0.9V_c$ the clusters are visible to $T \sim 2T_c$. The 'cluster survival scale' at V_c is $\sim 0.6T_c^0$ and drops slowly with increasing disorder.

Fig.2 shows spatial maps of the pairing field and the tunneling conductance, averaged over 100 thermal configurations, at strong disorder ($V = 0.9V_c$) for a single realisation of disorder. The Supplement shows results at weaker disorder. The top row shows $\langle|\Delta_i|\rangle$, normalised by the clean $T = 0$ value Δ_0. Next row: nearest neighbour averaged phase correlation $\Phi_i = \langle\frac{1}{4}\sum_\delta cos(\theta_i - \theta_{i+\delta})\rangle$, where δ refer to the four nearest neighbours of a site. Third row: $T_i^{gap} = \langle\int_{\omega_g^-}^{\omega_g^+} d\omega N_{ii}(\omega)\rangle$, the local tunneling conductance probed at subgap frequencies. Fourth row: T_i^{coh}. We set $\omega_g^- = 0$, $\omega_g^+ = 0.2t$. Columns, left to right, correspond to $T = 0$, T_c, $2T_c$.

Let us start with the patterns at $T = 0$, left column. (a). We see a clear separation between regions where $\langle|\Delta_i|\rangle \gtrsim 0.4\Delta_0$, and where $\langle|\Delta_i|\rangle \ll 0.4\Delta_0$. While there is significant variation in magnitude *within* the larger Δ regions, the distinction between large and small Δ regions

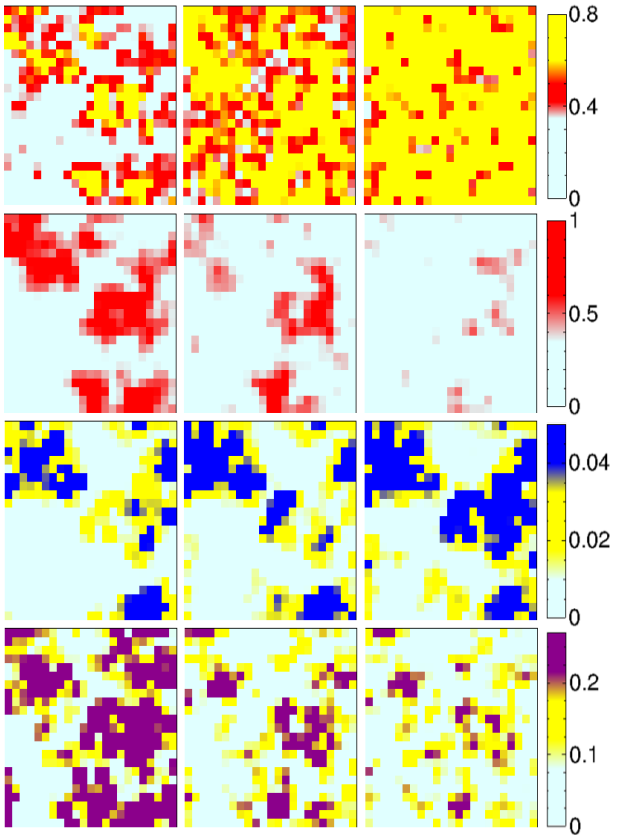

FIG. 2. Colour online: Spatial maps at $V = 0.9V_c$. 1st row: $\langle|\Delta_i|\rangle$, 2nd row: phase correlation Φ_i, 3rd row: tunneling conductance T_i^{gap}, 4th row: T_i^{coh}. The notation is explained in the text. Columns, from left to right, are for $T = 0$, T_c, $2T_c$. The interpretation of these patterns is discussed in the text.

is unambiguous. (b). The large Δ regions are phase correlated: Φ_i is large in regions where $\langle|\Delta_i|\rangle$ is large. These regions are the SC clusters. (c). T_i^{gap} shows that the large $\langle|\Delta_i|\rangle$ phase correlated regions have *large* subgap TC, while regions with poor SC correlation have virtually zero TC. This suggests a smaller local gap in the SC clusters, as we will confirm later, and a larger gap in the non SC regions. The behaviour is in contrast to homogeneous systems where larger $\langle|\Delta_i|\rangle$ would have meant a larger gap and a *smaller* TC. (d). The map for T_i^{coh} shows that the SC clusters in the ground state have a modest coherence peak, while there is no CP in the larger gap non SC regions. Overall, at $T = 0$ the non SC regions have no noticeable spectral weight from $\omega = 0$ to frequencies well beyond the average CP location.

Now the thermal evolution. By $T = T_c$, middle column, we observe the following. (a) There is significant homogenisation of $\langle|\Delta_i|\rangle$. Non SC regions generate a strikingly large $\langle|\Delta_i|\rangle$ while the SC clusters see a more modest growth from the $T = 0$ value. Temperature leads to strong spatially differentiated amplitude fluctuation in the system. (b) Φ_i shows thermal shrinking of the correlated regions. It is still large in parts of the regions which had the large $\langle|\Delta_i|\rangle$ at $T = 0$. The clusters are internally correlated but disconnected. The independent fluctuation of the phase of the different clusters leads to loss of global SC order. (c) There is no noticeable change in T_i^{gap} with T for regions that were non SC at $T = 0$. For SC regions there is an increase in intensity. (d) For T_i^{coh}, as we have already seen in Fig.1, areas with strong CP feature shrink but are still clearly visible. Non SC regions do not respond to temperature.

By $T = 2T_c$, 3rd column, (a) the mean magnitude has homogenised, with traces of clustering apparently lost, and (b) Φ_i is virtually zero everywhere. The homogenisation of amplitude and phase variables may suggest that any imprint of the $T = 0$ cluster pattern would be lost. However, (c) the subgap TC is still very inhomogeneous, but now uniformly large over regions that were SC at $T = 0$. So, even at this "high temperature" the subgap TC reveals the granularity of the ground state. Finally, (d) the high intensity regions in T_i^{coh} shrink and the pattern tends towards a homogeneous intermediate intensity with only small remnants of the high CP regions.

We have observed that at weaker disorder the correspondence of T_{gap}^i with the background superconducting pattern weakens. The data at $V = 0.5V_c$ in the Supplement show that there is no clear correspondence between T_{gap}^i and the correlated regions. T_{coh}^i, however, continues to roughly track the superconducting order, both in the ground state and at finite T, down to low disorder.

Fig.3 quantifies the distributions, $P(g)$ and $P(h)$, of gap magnitude and coherence peak integral, respectively, across the system. The results are for $V = 0.2V_c$ and $0.9V_c$, and $T/T_c(V) = 0,\ 0.5,\ 1.0$. At $0.2V_c$ the $P(g)$ has a mean $\approx 2\Delta_0$ at $T = 0$, with a narrow width around it.

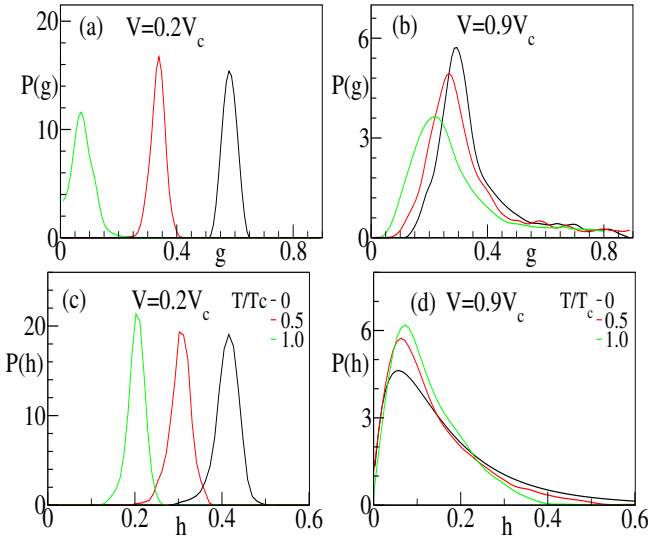

FIG. 3. Colour online: Thermal evolution of the gap and coherence peak height distribution. Top: Gap distribution for $V = 0.2V_c$ (left) and $0.9V_c$ (right). Bottom: Coherence peak height distribution at same V. $T/T_c(V) = 0, 0.5, 1.0$.

With increasing T the mean 'gap' shifts to lower values while the width shows a small increase. This suggests a homogeneous decrease throughout the system. At $0.9V_c$ $P(g)$ is wide at $T = 0$ with a large gap tail arising from sites with large positive or negative effective potential (we call these hill and valley sites). Increasing T leads to shift in weight to lower g from intermediate values while $P(g)$ at large g remains unaffected.

Coming to $P(h)$, panel (c) shows that the coherence peak distribution is also roughly uniform at $0.2V_c$ at all T. The peak at $h \gtrsim 0.4$ at $T = 0$ narrows slightly and moves to lower values at higher T but the mean remains finite since we have not subtracted the high T background. At $0.9V_c$, however, most sites have poor coherence features, defining the trunk of the distribution, except for the tail with $h \gtrsim 0.4$ arising from sites in the superconducting clusters. With increasing T as the SC regions shrink the weight in this $h \gtrsim 0.4$ region is lost.

Fig.4 correlates the low energy features of local gap and coherence peak to spectral weight distribution over a wider frequency window. We plot the LDOS at two representative sites ('plateau' and 'hill') at low and high disorder. The plateau site involves an effective potential $V_i - \phi_i$ close to the mean value, and a local density n_i close to the average, $n_{av} \sim 0.9$, while the hill site has a large positive effective potential and $n_i \ll n_{av}$. At low disorder, Fig.4(a)-(b), both sites show coherence peaks and similar gaps, with the hill site naturally having larger weight at $\omega > 0$. The thermal evolution is also similar, with both gaps decreasing and closing at $T \lesssim T_c$.

At high disorder, Fig.4(c)-(d), the LDOS at the plateau site (part of a SC cluster) shows a narrow gap at low T, moderate coherence peaks, and expected thermal be-

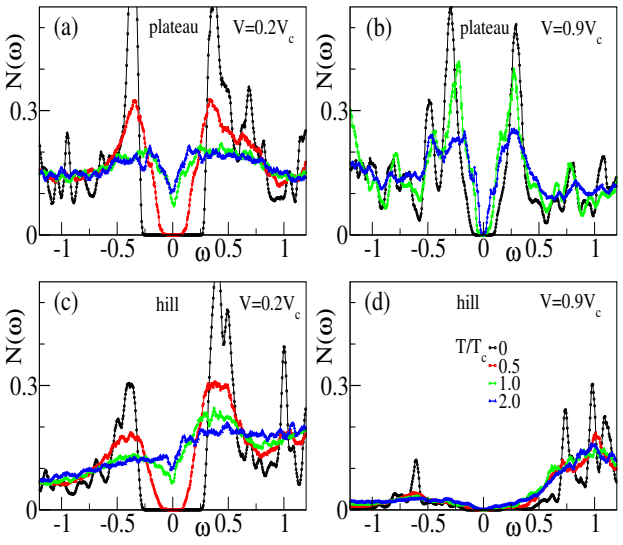

FIG. 4. Colour online: Local DOS on a typical 'plateau' site (top) and 'hill' site (bottom). The left panels (a) & (c) are at $V = 0.2V_c$, the right panels (b) & (d) are for $V = 0.9V_c$. In each panel the low energy DOS is shown for four temperatures $T \approx 0,\ 0.5T_c,\ T_c,\ 2.0T_c$. The curve at $0.5T_c$ has been omitted in (b) for clarity.

haviour. The hill site, by contrast, shows a large gap (strongly suppressed low frequency spectral weight), no coherence peaks, and is virtually insensitive to T.

We now discuss the multiple scales that emerge in the strongly disordered superconductor, and the relevance of our results to recent STS measurements.

(i) *Multiple scales:* In the clean limit, weak coupling SC is characterised by only one scale, $T_c^0(U)$, while strong coupling brings into play two additional [25] scales $T_g^0(U) > T_c^0(U)$ and $T_{pg}^0(U) > T_g^0(U)$. This paper focuses on the weak coupling end where there is no gap/PG above T_c at $V = 0$ but disorder *generates* such scales. These scales emerge due to the fragmentation of the SC ground state with increasing disorder (the nature of the patterns is discussed in the Supplement, and also [16]). The inhomogeneous state leads to a spatially varying phase and amplitude stiffness, whose distribution and spatial correlation dictates the thermal response.

The Supplement describes how a bond resolved phase stiffness, J_{ij}, can be extracted from the non local pairing susceptibility in the disordered ground state. Focusing on nearest neighbour bonds, at small V the J_{ij} are 'large', homogeneous, and $\sim \mathcal{O}(J_0)$, the clean value. At large V they are strongly inhomogeneous, with a smaller mean value $\langle J\rangle \ll J_0$. While $\langle J\rangle$ (on the percolative backbone) decides $T_c(V)$, the presence of bonds with $J \sim J_0 \gg \langle J\rangle$, near the center of the SC clusters, leads to survival of local SC correlations to $T_{clust} \gg T_c$ as $V \to V_c$. The Supplement shows plots of the distribution $P(J_{ij}, V)$ and a spatial map of J_{ij} at stong disorder.

Although phase fluctuations destroy global order, the $|\Delta_i|$ survive to $T \gg T_c$. At $U = 2t$ this sustains a gap to $T_g > T_c$ and then a PG to a scale $T_{pg} > T_g$, ultimately closing due to amplitude fluctuations. The Supplement shows these scales at $U = 2t$, and also $U = 4t$ to allow extrapolation over a wider interaction window. At $U = 2t$, while $T_c \to 0$ as $V \to V_c$, T_{clust} remains roughly constant at $\sim 0.5T_c^0$, as does T_g. T_{pg} is much larger than these scales. At $U = 4t$ $T_g \gg T_{clust}$, so their coincidence at $U = 2t$ is accidental. Extrapolating downward we expect that when $U \ll t$, T_{clust} will continue to be a finite fraction of T_c^0, with $T_{pg} \sim T_{clust}$.

Comparison with experiments: Our main results, *i.e*, the emergence of a T_{clust}, T_g, *etc*, in addition to T_c, the shrinkage and fragmentation of the SC pattern with increasing temperature, and the distinct thermal evolution of the STS spectra in the SC and insulating regions, are all in agreement with recent experiments. However, there are also important differences, arising from (i) our parameter choice, (ii) our approximation, and (iii) the neglect of Coulomb interactions. (i) Experimental spectra indicates a pseudogap [12], rather than a hard gap above T_c for $V \to V_c$. Our exploration of the U dependence suggests that at weaker coupling such a result would emerge from our method as well. Another effect of the relatively 'large' coupling that we use is the larger variation of local gaps between the SC and insulating regions, experimentally these gaps are comparable [10]. (ii) The neglect of quantum fluctuations in our treatment of the A2DHM prevents access to the correct asymptotic low temperature behaviour for $V \to V_c$. However, apart from the immediate vicinity of V_c the thermal fluctuations seem to capture most of the qualitative experimental features. (iii) The recent observation [14] of enhanced zero-bias conductance in the insulating regions is probably caused by additional interactions that are absent in our model. Also, the broad V-shaped background observed in the STS spectra possibly arises from Coulomb interactions, and is absent in our results.

Conclusions: We have studied the spatial signatures of the thermal transition in a disordered s-wave superconductor as probed by tunneling spectroscopy. Our detailed spatial maps of the coherence and subgap features in the local DOS allow us to identify the distinct evolution of the superconducting and 'insulating' regions with temperature. We point out new thermal scales, T_{clust}, T_{pg} and T_g that come into existence at strong disorder, identify their physical origin, and quantify their dependence on disorder and interaction strength. Recent experiments have already indicated the existence of such scales in 2D films, our results provide the broader framework within which these results can be analysed.

Acknowledgments: We acknowledge use of the High Performance Computing Cluster at HRI. PM acknowledges support from a DAE-SRC Outstanding Research Investigator Award, and the DST India (Athena). We thank Amit Ghosal and P. Raychaudhuri for discussions.

[1] P. W. Anderson, J. Phys. Chem. Solids **11**, 26 195921

[2] A. A. Abrikosov and L. P. Gorkov, Zh. Eksp. Teor. Fiz. **36**, 319 (1959)

[3] For reviews, see A. M. Goldman and N. Markovic, Phys. Today **51**, No 11, 39 (1998), D. Belitz and T. Kirkpatrick, Rev. Mod. Phys. **66**, 261 (1994), M. V. Sadovskii, Phys. Rep. 282, 225 (1997), V. F. Gantmakher and V. T. Dolgopolov, Phys. Usp. **53**, 3-53 (2010).

[4] D. B. Haviland, Y. Liu and A. M. Goldman, Phys. Rev. Lett. **62**, 2180 (1989).

[5] D. Shahar and Z. Ovadyahu, Phys. Rev. B **46**, 10917 (1992).

[6] W. Escoffier, *et al.*, Phys. Rev. Lett. **93**, 217005 (2004).

[7] T. I. Baturina, *et al.*, Phys. Rev. Lett. **99**, 257003 (2007).

[8] B. Sacepe, *et al.*, Phys. Rev. Lett. **101**, 157006 (2008).

[9] B. Sacepe, *et al.*, Nature Commun. **1**, 140 (2010).

[10] B. Sacepe, *et al.*, Nature Phys. **7**, 239 (2011).

[11] M. Mondal, *et al.*, Phys. Rev. Lett. **106**, 047001 (2011).

[12] M. Chand, *et al.*, Phys. Rev. B **85**, 014503 (2012).

[13] Y. Noat, *et al.*, arXiv:1205.3408.

[14] A. Kamlapure, *et al.*, Sci. Rep. **3**, 2979 (2013)

[15] D. Sherman, *et al.*, Phys. Rev. Lett. **108**, 177006 (2012).

[16] A. Ghosal, M. Randeria and N. Trivedi, Phy. Rev. B **65**, 014501 (2001)

[17] N. Trivedi, R. T. Scalettar and M. Randeria, Phys. Rev. B **54**, 3756 (1996).

[18] K. Bouadim, Y. L. Loh, M. Randeria and N. Trivedi, Nat. Phys. **7**, 884 (2011)

[19] Y. Dubi, Y. Meir and Y. Avishai, Nature, **449**, 876 (2007).

[20] M. Mayr, G. Alvarez, C.Sen and E.Dagotto, Phys. Rev. Lett. **94**, 217001 (2005).

[21] S. Kumar and P. Majumdar, Eur. Phys. J. B, **50**, 571 (2006).

[22] S. Tarat and P. Majumdar, Europhys. Lett. 105 (2014) 67002.

[23] S. Tarat and P. Majumdar, arXiv:1402.0817.

[24] There is no SIT in the ground state strictly within HF-BdG theory. However at any finite T phase fluctuations lead to a finite $V_c(T)$. Our V_c is an extrapolation of this quantity [22].

[25] Note that unlike T_c, the gap and pseudogap vanishing scales are more ambiguous, particularly the later. Nevertheless, they are useful constructs, and at least in the present case can be reasonably estimated.

Supplementary material for "Tunneling Spectroscopy Across the Superconductor-Insulator Thermal Transition"

Sabyasachi Tarat and Pinaki Majumdar

arXiv:1406.5423v1 [cond-mat.str-el] 20 Jun 2014

COMPUTATION OF MEASURABLES

In our scheme, the local density of states (LDOS) is given by

$$N_{ii}(\omega) = \frac{1}{N}\sum_n \langle (|u_n^i|^2\delta(\omega - E_n) + |v_n^i|^2\delta(\omega + E_n))\rangle$$

where the u_n, v_n are obtained from the BdG eigenfunctions, E_n is the positive BdG eigenvalue, and the entire expression is thermally averaged (angular brackets) over equilibrium configurations of the auxiliary field. We typically average over ~ 100 configurations at a given temperature. The third row in Fig.2 corresponds to LDOS averaged over the interval $\delta\omega_{gap} = [0, 0.15]t$, and the fourth row to $\delta\omega_{coh} = [0.15, 0.35]t$.

The global DOS of the quasiparticles is obtained as $N(\omega) = \langle \sum_n \delta(\omega - E_n)\rangle$, where now the sum runs over both positive and negative E_n. The quasiparticle (QP) gap is the minimum of $2E_n$ over all thermal configurations at a given T.

CLUSTER PATTERN AT $T = 0$

Fig.S1 shows 'gap-maps' for a particular disorder realisation at $V = 0.9V_c$ for three different cases: (a) actual ground state, (b) ground state obtained with $V_i^{eff} = V_i - \phi_i$ and (c) with V_i, but the potential scaled to lie between $(V - (U/2)n_{min}, -V - (U/2)n_{max})$, with $n_{min} = 0$ and $n_{max} = 2$. The 'gap' at a site 'i' is defined as the difference between the smallest energy $\omega_+ > 0$ at which the LDOS $N_{ii}(\omega) \gtrsim N_{cut}$ and the corresponding $\omega_- < 0$, where N_{cut} is a suitably defined cutoff.

All three show the same pattern of low gap areas (coloured red) even though the overall scales change. Thus, superconducting clusters form in areas that are already defined by a small local gap at the Fermi level. The Hartree field magnifies this effect, further increasing the local gaps in the insulating regions, while the Δ open up a smaller gap on sites within the superconducting clusters.

Since regions with low local gap *around the chemical potential* decide the cluster pattern, this pattern depends sensitively on the overall electron density in the system.

To understand the density distribution in the system we define 'hill' sites as those with $n_i \lesssim 0.4$, valley sites as those with $n_i \gtrsim 1.6$, and 'plateau' sites where n_i is within 10% of $n_{avg} \sim 0.9$ The rest are 'moderate' sites. Fig.S2 shows the distribution of 'plateau' sites inside the SC clusters (with $\Delta \gtrsim 0.4\Delta_0$) as well as outside at high disorder $V = 0.9V_c$. The plots clearly show that a majority of the plateau sites lie inside the SC cluster region, providing a backbone for the formation of the clusters.

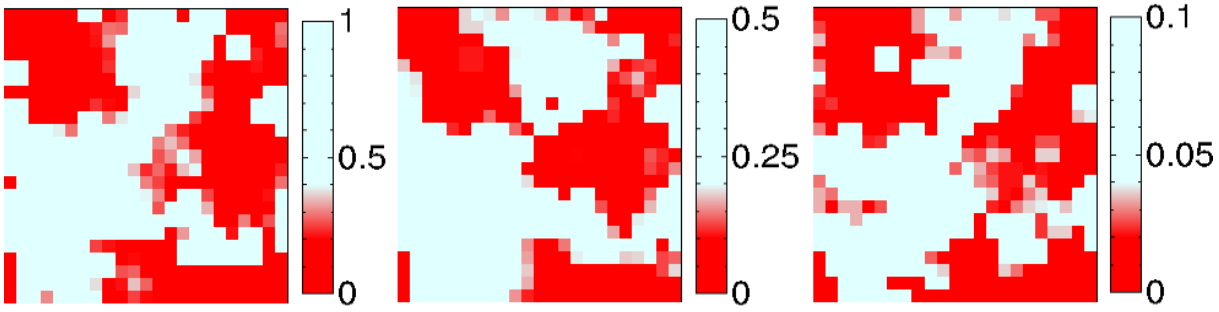

Figure S1. Colour online: Gap maps for 3 cases, $T = 0$. Left: Original calculation, showing patches with low gaps, idential to the correlated patches. Middle: With V_{bare}, scaled to lie between $(-V - 2, V)$, showing low gap patches with same basic structure; Right: with V_{eff}, increasing the contrast of the original V, gives similar map, with gaps of the insulating regions raised substantially.

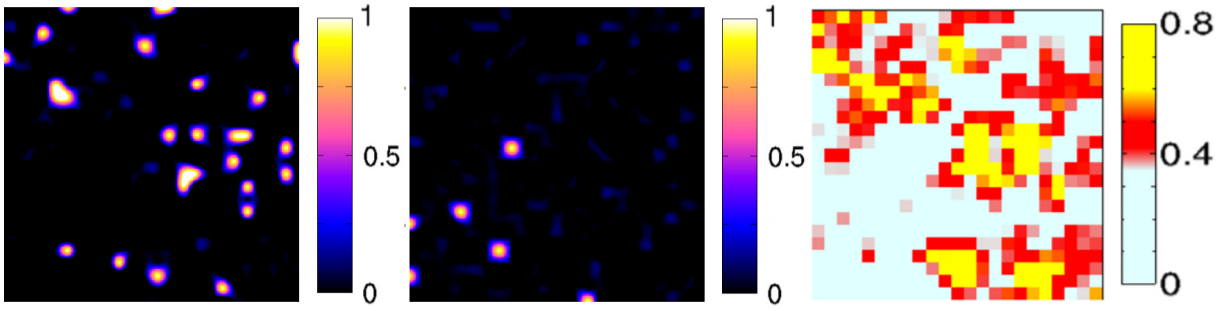

Figure S2. Colour online: Comparison of location of 'plateau' sites (see text) inside superconducting clusters (left) with the same outside clusters (middle) at $V = 0.9V_c$, $T = 0$. Right figure shows the spatial plot of $|\Delta_i|$ for reference. 'Pleateau' sites form a backbone over which the superconducting clusters are formed. In the insulating area, 'hill' or 'valley' sites (see text) predominate, ruling out the formation of SC clusters.

These only account for 13% of the total number of sites, but combined with the 40% 'moderate' sites, they allow enough particle-hole mixing to favour the formation of SC clusters. The fact that 47% *of sites within the SC clusters* are of the 'hill/valley' type shows that the SC regions are far from being 'flat'. On the other hand, in the insulating regions, 80% of the sites are of the 'hill/valley' type, surrounding the few isolated 'plateau' site.

SPATIAL PATTERNS AT MODERATE DISORDER

In the main text we have discussed the strong disorder regime where, for the system size we are studying, the cluster pattern is quite prominent. At weaker disorder the patterns are more ambiguous, and we discuss this $V = 0.5V_c$ case here.

Ground state: The top left panel in Fig.S3 is the $T = 0$ pattern of $\langle|\Delta_i|\rangle$. In contrast to $0.9V_c$ in the main text this has only small regions with suppressed amplitude, scattered in a background with moderate to large $\langle|\Delta_i|\rangle$. The corresponding nearest neighbour phase correlation Φ_i is almost saturated over the system, except for small regions which correlate with the small $\langle|\Delta_i|\rangle$ patches.

The subgap tunneling *does not* follow the trend observed at $0.9V_c$: T_i^{gap} seems to be larger where $\langle|\Delta_i|\rangle$ is either weak or only moderately large. There is no direct correspondence with the correlated regions. Local gaps in the correlated region can be larger as well as smaller than gaps in poorly correlated regions, but we observe a partial recovery of the 'large $\Delta \equiv$ large gap' rule. T_i^{coh} is large over most of the system, with larger intensity corresponding, roughly, to larger values of $\langle|\Delta_i|\rangle$.

Thermal evolution: The middle column in the right set of panels is for $T \approx 0.5T_c$ and the right column for $T \approx T_c$. The $\langle|\Delta_i|\rangle$ increase on an average with T and is uniform by $T \approx T_c$. The loss of phase correlation is spatially differentiated, stronger phase correlation survives in regions where the $\langle|\Delta_i|\rangle$ is larger. By T_c the $\langle|\Delta_i|\rangle$ has homogenised and phase correlations are lost throughout, unlike the strong disorder case where correlated patches survived to $\sim 1.3T_c$.

The subgap tunneling does not have a forceful correspondence with the profile of $\langle|\Delta_i|\rangle$ or Φ_i. At $T = 0.5T_c$ it seems to show low intensity (hence larger 'gap') roughly in regions which have larger $\langle|\Delta_i|\rangle$ and stronger Φ_i (roughly the ring like region excluding the center). At $T \sim T_c$ the intensity is large almost everywhere and no signature of any cluster can be seen. Large intensity in T_i^{coh} at $T = 0.5T_c$ similarly has a rough correspondence with large $\langle|\Delta_i|\rangle$ and phase correlation and only a tentative match with Φ_i at $T \sim T_c$.

EFFECTIVE GINZBURG-LANDAU FUNCTIONAL

The interplay of 'amplitude' and 'phase' fluctuations in our model is best understood in terms of a simple lattice Landau-Ginzburg model:

$$\mathcal{F}(\Delta) = \sum_{i \neq j} J_{ij}\Delta_i\Delta_j^* + \sum_i (a_i|\Delta_i|^2 + b_i|\Delta_i|^4) \tag{1}$$

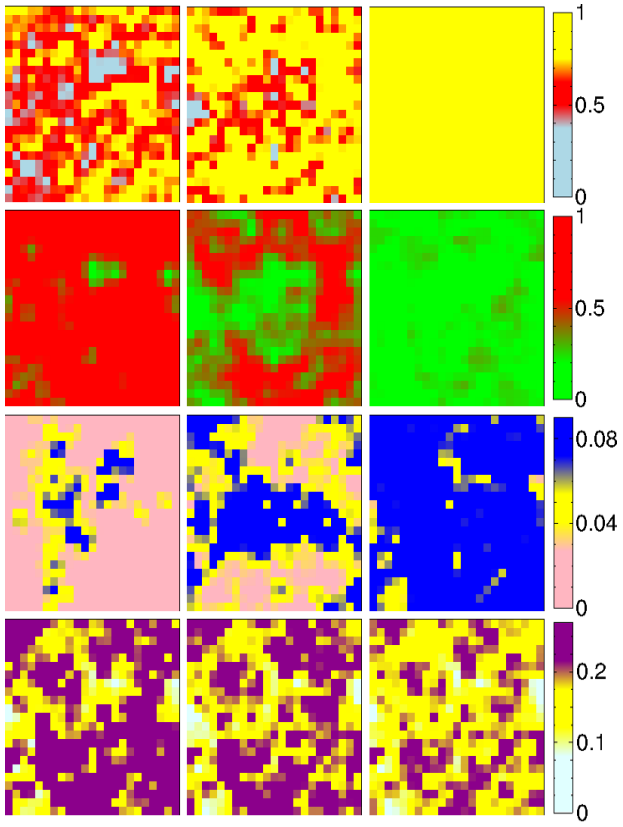

Figure S3. Colour online: Spatial maps at $U = 2$ and $V = 0.5V_c$. First row: $\langle|\Delta_i|\rangle$, second row: phase correlation Φ_i (see text), third and fourth rows show the tunneling conductance averaged over two frequency (or bias) windows ω_{gap} and ω_{coh}. Along the row: temperatures $T = 0$, $0.4T_{c0}$ and $0.8T_{c0}$. $\langle|\Delta_i|\rangle$ at low T forms phase correlated clusters, which shrink in size as T is increased. $\langle|\Delta_i|\rangle$ is weakly inhomogeneous at low T, and smoothens with increasing T. Φ_i decrease with T and vanishes almost homogeneously at T_c (not shown, but between $0.5T_{c0}$ and T_{c0}.) The subgap region lights up with increasing T, due to the transfer of spectral weight to low frequency, while the plot for ω_{coh} loses intensity.

The a_i and b_i, crudely, control the $|\Delta_i|$ while J_{ij} determine a bond coupling between the 'i' and 'j' sites (not necessarily nearest neighbours). These parameters are in general temperature dependent, and the clean problem at $U = 2t$ involves renormalisation of all these parameters with temperature. We focus here on understanding the strong disorder regime $V \gtrsim 0.75V_c$ and the thermal evolution of the superconducting clusters only over a small temperature window above the ground state (the T_c here is small). Such a situation allows us to ignore the thermal renormalisation of the GL parameters as a first approximation.

We calculate J_{ij} via a perturbative expansion of the energy in Δ_i around the disordered ground state. This leads to: $J_{ij} \sim \frac{1}{\beta}\sum_n G_{ij}(i\omega_n)G_{ij}(-i\omega_n)$ where $G_{ij}(i\omega_n)$ is the electronic Greens function computed in the background defined by V_i and ϕ_i. We compute G_{ij} exactly in the $\{V_i + \phi_i\}$ background. The a_i and b_i can be found by fitting the local amplitude distributions to the given form, but we concentrate on J_{ij} here.

Fig.S4 compares the phase correlations obtained from the bond disordered XY model, above, with that from the full Monte Carlo at $V = 0.8V_c$. We find a reasonable match.

Fig.S5 shows the distribution of the nearest neighbour J_{ij} at various disorder values and a spatial map of the same at strong disorder, $V = 0.9V_c$. The distributions broaden with increasing disorder, and their means shift to lower values, but a finite proportion of sites have $J \sim J_0$ even at large disorder, where J_0 is the clean value ~ 0.023. These correlations thus only vanish when $T \sim J\Delta^2$, where Δ is typically a large fraction of the clean Δ_0, explaining why $T_{clust} >> T_c$ even at large disorder. A comparison of the J_{ij} map with the low temperature correlation map in Fig.S4 clearly shows that SC clusters generally have larger J_{ij}, with the middle of the clusters having the largest stiffnesses. Thus, under thermal evolution, these regions are the last to vanish.

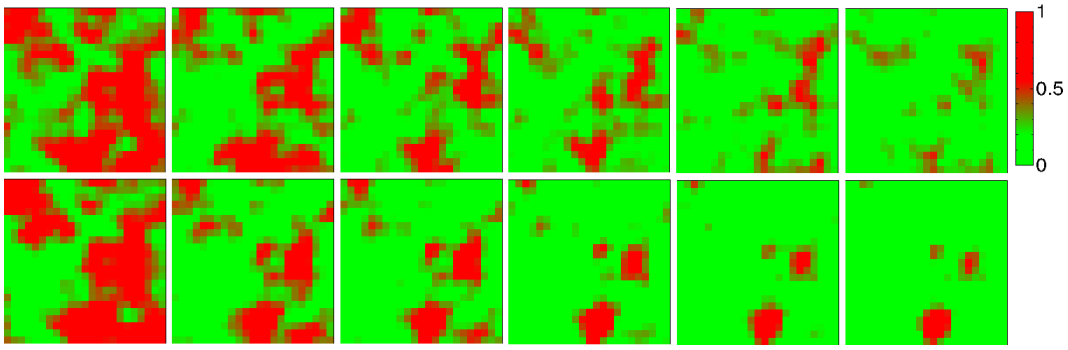

Figure S4. Colour online: Comparison of correlated patches for $V = 0.8V_c$ for successive T points using the full Monte Carlo (top) and the simplified XY model (bottom). The basic phenomenon of an island pattern at low T, and shrinkage of these clusters with increasing temperature is well captured by the simplified model.

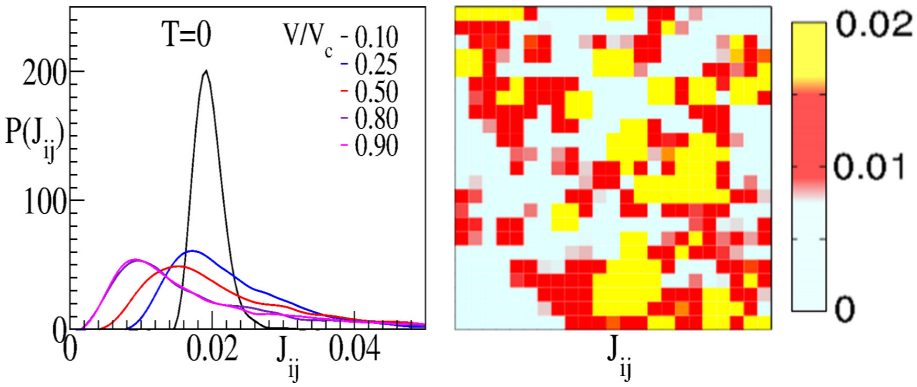

Figure S5. Left: Distribution of nearest neighbour J_{ij} at different disorder, showing successive broadening with disorder, but even at strong disorder, a finite number of sites have $J \sim O(J_0)$. Right: Spatial map of J_{ij}, at $V = 0.9V_c$, showing that the large values of J_{ij} correspond to the centres of the SC clusters.

DEPENDENCE OF TEMPERATURE SCALES ON DISORDER AND COUPLING

Fig.S6 shows the phase diagrams for $U = 2$ and 4. The tails emphasize the fact that in principle, the $T = 0$ state is always superconducting within our scheme. The increased Hartree field at stronger coupling increases the effective disorder $V_i - \phi_i$, leading to a smaller V_c. This also leads to a faster fragmentation with disorder, and a more differentiated J_{ij} distribution, which results in a faster decline in T_{clust} at $U = 4$ compared to that at $U = 2$. The gap vanishing scale, on the other hand, increases considerably with coupling, and at $U = 4$, it is greater than the clean T_c^0 at all disorder values considered here. Thus, the similar magnitudes for T_{clust} and T_g observed in experiments is only seen at weak coupling ($U = 2$), and is not true in general.

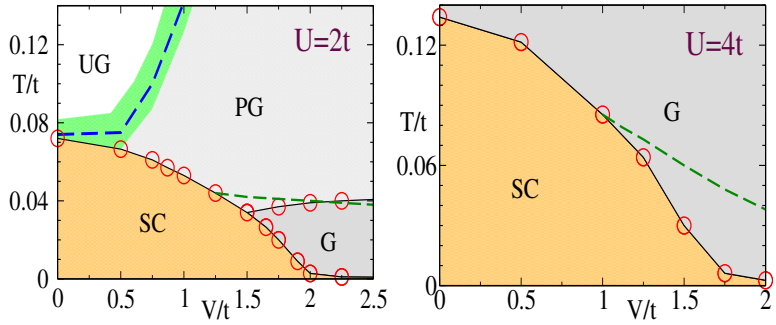

Figure S6. Colour online: Phase diagrams showing superconducting (SC), gapped (G), pseudogapped (PG) and ungapped (UG) phases, and the cluster vanishing scale T_{clust} (green dashed lines) at $U = 2$ and 4 (see text).